UDC 544.032.4+544.015

DOI: 10.15372/CSD2020264

Nanostructured Composites MWCNT/Transition Metal Oxide Obtained by Thermal Decomposition of Hydroxides

T. A. LARICHEV[1], YU. A. ZAKHAROV[1,2], N. M. FEDOROVA[1], G. YU. SIMENYUK[2], V. M. PUGACHEV[2], YU. V. LOKTIONOV[1], V. E. NIKIFOROV[1]

[1]*Kemerovo State University, Kemerovo, Russia*

E-mail: timlar@kemsu.ru

[2]*Federal Research Center for Coal and Coal Chemistry, Siberian Branch, Russian Academy of Sciences, Kemerovo, Russia*

Abstract

The structural, morphological and electrochemical properties of nanocomposite materials obtained by thermal decomposition of cobalt hydroxides and mixed cobalt-zinc hydroxides on the surface of a carbon matrix formed by multi-walled carbon nanotubes (MWCNT) were investigated. The interaction of the solutions of cobalt and zinc sulphates with sodium hydroxide results in the formation of the solid phase which includes cobalt hydroxide and zinc oxide. Subsequent thermal treatment in the air leads mainly to the formation of zinc cobaltate $Zn_xCo_{(1-x)}O_y$, in which the relative content of cobalt and zinc can vary within a broad range. The electrochemical properties of synthesized nanocomposite materials were investigated by cyclic voltammetry. Investigation of the electrochemical properties of the synthesized nanocomposite materials by means of cyclic voltammetry showed that the introduction of cobalt oxide into carbon matrix causes an increase in electrical capacitance within the whole range of potential scanning rates (10–80 mV/s). Application of electrode materials based on the carbon/zinc cobaltate composite for manufacture allows an increase in specific capacitance of supercapacitors by a factor of 1.5 and saves cobalt, a material in short supply.

Keywords: zinc cobaltate, cobalt oxides, cobalt hydroxide, zinc hydroxide, carbon nanotubes, nanocomposites

INTRODUCTION

The development of an electricity supply system is impossible without the application of efficient systems of electric power accumulation and transformation. The key nodes of these systems may be supercapacitors (ionistors) distinguished by the high rate of the charging-discharging cycle and, as a consequence, the ability to give the accumulated energy out in the form of electric current of high power [1]. Substantial progress has been observed during recent years in the area of the development of supercapacitor technologies, which is first of all connected with the improvement of the materials used to manufacture electrodes. The attention of researchers is attracted by the possibilities to use nanocomposite electrode materials based on the current-conducting highly porous matrix (usually carbon) with intercalated nanoparticles of the compounds of metals with variable valence (oxides, sulphides, nitrides, etc.) [2]. A combination of the materials of this kind provides an increase in the amount of accumulated electric capacitance due to an increase in the specific surface area for charge accumulation, mainly due to oxidation-reduction (Faraday) processes in the filler of the composite (so-called pseudo-capacity component).

However, the synthesis of nanocomposites combining different allotropic and morphological kinds of carbon (carbon single- and multiwall nanotubes, graphene, fullerenes, etc.) and nanometer-

sized particles of inorganic compounds with prescribed particle size and morphology with regulated distribution over the surface of carbon matrix (including its pores) appears to be a difficult task. The methods used to develop the structures of this kind include solvothermal and sol-gel methods, the methods of chemical, electrochemical and electrophoretic deposition etc. [3, 4]. In the present work, we apply a known method involving the deposition of hydroxides of transition metals (intermediate products) on the surface of the carbon matrix followed by their transformation into the target oxide by means of thermal treatment (TT) to obtain the fillers for nanocomposites [5].

Multiwall carbon nanotubes (MWCNT) synthesized at the Boreskov Institute of Catalysis SB RAS (Novosibirsk) were used as the carbon matrix. The characteristics of MWCNT [6], namely narrow distribution over channel diameter (2–5 nm), external diameter (18–21 nm); the almost complete absence of impurities after washing (in particular, the absence of the catalysts of synthesis); very low microporosity (0.03 cm^3/g) in combination with moderate mesoporosity (0.70–0.77 cm^3/g) connected mainly with the channels and well reproducible, – allow us to consider this carbon matrix as a convenient model for the investigation of the properties of nanostructured composites (NC) obtained on this basis.

Hydroxide fillers for these NC are often prepared using the precipitation of metal hydroxides or carbonated by carbamide (urea) [7–10]. Carbamide in the aqueous solution undergoes slow hydrolysis:

$$CO(NH_2)_2 + 3H_2O \rightarrow 2NH_4OH + CO_2 \quad (1)$$

Hydrolysis is accompanied by a slow increase in pH within the entire solution volume [11]. If multi-charged ions of transition metals are present in the solution, hydrolysis reactions leading to the formation of precipitate are initiated, though there is no substantial local supersaturation. In turn, this creates the conditions for the formation of a large amount of fine solid particles which are rather uniform in size [12]. Since hydrolysis results in the formation of both the base (NH_4OH) and carbonate component (CO_2), precipitation by carbamide may lead to the formation of hydroxides, carbonates, and basic carbonates of metals. It should also be stressed that the salts of cobalt (II) may form complex compounds with carbamide, characterized by different composition and stability [13]. The majority of these compounds are decomposed into initial components in aqueous solutions.

So, the assumed hydrothermal reaction proceeding in the presence of carbamide in solution may be represented as follows:

$$CoCl_2 + 2CO(NH_2)_2 + H_2O \rightarrow Co_2(OH)_2CO_3 + 2NH_4Cl + CO_2 \quad (2)$$

With an increase in solution temperature, carbamide hydrolysis is accelerated; the side products of hydrolysis are volatile and leave the solution rather rapidly. For instance, at a temperature of 96–98 °C, ammonium carbonates are decomposed, and CO_2 leaves the system [12], which hinders the formation of hydroxycarbonates in the reactions involving precipitation with carbamide. Relying on this fact, it is reasonable to carry out the synthesis in an open system at the temperature of the start of carbamide hydrolysis, which is equal to 80 °C.

During recent years, it is increasingly frequently proposed to use the phases of complicated composition containing mixed or doped oxides as the oxide material in electrode nanocomposites. These oxides possess advantages from the viewpoint of electric conductivity, the ability to accumulate electric charge, etc. [14]. For example, zinc cobaltate ($ZnCo_2O_4$) is considered a promising filler [15]. The additional positive effect is achieved in this case due to the fact that two different transition metals may form a mixed oxide with more attractive electrochemical characteristics and increased stability in comparison with the systems based on monometallic materials. In addition, the replacement of some metal cations in cobalt oxide may produce the effect of a decrease in strain/deformations arising during long-term charge-discharge [16]. It is also remarkable that $ZnCo_2O_4$ possesses much higher electric conductivity and electrochemical activity than many ordinary binary oxides of transition metals. This increase in conductivity allows a substantial increase in the capacity characteristics of supercapacitors.

To evaluate the outlooks of the above-described approaches, in the present work we considered the possibility to obtain NC based on carbon matrix (MWCNT), which is proposed as the model, with the fillers of two types: 1) cobalt (II, III) oxide obtained by thermal decomposition of the products of hydrolysis of cobalt salts in the presence of carbamide; 2) a mixed cobalt-zinc oxide obtained as a result of thermal decomposition of the mixed cobalt-zinc hydroxide, and investigated the properties of thus prepared NC.

EXPERIMENTAL

Reagents and materials

Reagents used to prepare solutions were not lower than Ch. D. A. reagent grade (pure for analysis).

Preparation of MWCNT/Co_3O_4 composite

MWCNT in the amount of 0.2 g was added to a 5 % carbamide solution in distilled water, then the mixture was heated to 80 °C, and the required volume of cobalt chloride solution was added (depending on the necessary content of cobalt as the element in the NC).

The hydrolysis of carbamide in the presence of cobalt chloride solution was carried out under mixing and keeping the volume of the reaction mixture constant. The total time of synthesis was 2 h. After the synthesis, the cooled mixture was filtered with a Buchner funnel using a water-jet pump.

The precipitate collected from the filter was dried at room temperature to the constant mass. The assumed composition of the composite obtained at this stage (B13–B15 samples) is MWCNT/$Co_2(OH)_2CO_3$.

Thermal treatment of the intermediate product was carried out in a thermal box Tulyachka 2 (Russia) for 180 min at 300 °C in air. The final composite material (B13.1–B15.1 samples) was a black loose powder. The expected composition of the obtained NC samples before and after TT is shown in Table 1.

Preparation of MWCNT/Znx$Co_{(1-x)}O_y$ composite ($x < 1$, $y \le 1.5$)

Four NC samples were manufactured: MWCNT-type carbon material (0.2 g) was used as the matrix, and the filler deposited on its surface was mixed cobalt-zinc hydroxide with the calculated molar fraction of cobalt 0.90, 0.75, 0.50, 0.25 in the filler and with the mass content of metals in the composite 10 mass %.

TABLE 1

Expected composition of the composite materials

Sample	Expected composition of the composite	Calculated content of Co in nanocomposite, mass %
B13	MWCNT/$Co_2(OH)_2CO_3$	5
B14	MWCNT/$Co_2(OH)_2CO_3$	10
B15	MWCNT/$Co_2(OH)_2CO_3$	15
B13.1	MWCNT/Co_3O_4	5
B14.1	MWCNT/Co_3O_4	10
B15.1	MWCNT/Co_3O_4	15

To prepare the composite material, weighted portions of MWCNT were transferred into a weighing bottle. The solutions of cobalt sulphate and zinc sulphate were mixed in the required proportions (their total volume was 1 mL). The carbon matrix was impregnated with this solution in the weighing bottle for 1 h. After impregnation, the solution of NaOH was added in the calculated amounts into the bottle to obtain cobalt-zinc hydroxide according to the exchange reaction

$$x\mathrm{ZnSO_4} + (1 - x)\mathrm{CoSO_4} + 2\mathrm{NaOH} \rightarrow \mathrm{Zn}_x\mathrm{Co}_{(1-x)}(\mathrm{OH})_2 + \mathrm{Na_2SO_4} \quad (3)$$

Thus obtained composite material (M1, M2, M3, M4 samples with the molar fraction of cobalt in the filler 0.90, 0.75, 0.50, 0.25, respectively) was transferred to the paper filter of Buchner funnel conjugated with Bunsen flask, washed with distilled water from sodium sulphate, and dried under vacuum at room temperature.

Thermal treatment of the obtained intermediate product of NC was carried out in Tulyachka 2 thermal box in the air in two stages: 1) 60 min at 120 °C; 2) 240 min at 300 °C. As a result of TT, M1.1–M4.1 NC samples were obtained, with assumed composition MWCNT/$Zn_xCo_{(1-x)}O_y$ ($x < 1$, $y \le 1.5$). Sample characteristics before and after TT controlled by synthesis conditions and confirmed by the data of X-ray fluorescence analysis (XFlA) are presented in Table 2.

Methods of investigation

The elemental composition of the samples was determined by means of optical emission spectrometry with inductively coupled plasma (OES) with the help of an iCAP 6500 DUO spectrometer (Thermo Scientific, Great Britain). The portions of preliminarily prepared NC samples (10–20 mg each) were poured with 5 ml of a mixture of hydrochloric and nitric acids (3 : 1). Tightly closed high-pressure polymer tubes with the mixture of reagents were placed in the thermal unit, heated to 80 °C, kept under these conditions for 2 h, and then cooled to room temperature. The mixtures were diluted to the volume prescribed by the procedure, and centrifuged to separate the precipitate. The filtrate was subjected to analytical investigation.

The structures of the obtained NC samples were studied by means of X-ray diffraction analy-

TABLE 2

Characteristics of samples of the MWCNT/$Zn_xCo_{(1-x)}O_y$ ($x < 1$, $y \le 1.5$) before thermal treatment (TT) (M1–M4) and after it (M1.1–M4.1)

Sample	Ratio of Co/Zn molar fractions			Composite mass, mg		Mass loss during TT, mg
	predetermined during synthesis	according to the data of XFlA[a]				
		before TT	after TT	before TT	after TT	
M1	0.90/0.10	0.89/0.11		194.8		12.5
M1.1			0.92/0.08		182.3	
M2	0.75/0.25	0.74/0.26		119.9		12.2
M2.1			0.71/0.29		107.7	
M3	0.50/0.50	0.55/0.45		183.1		15.0
M3.1			0.52/0.48		168.1	
M4	0.25/0.75	0.23/0.77		176.8		21.2
M4.1			0.22/0.78		155.6	

[a]XFlA is X-ray fluorescence analysis.

sis (XRD) and X-ray fluorescence analysis (XFlA) with the help of a Difrey-401 diffractometer (Russia) equipped with a tube with the iron anode ($\lambda_{K\alpha}$ = 1.9373 Å) and energy-dispersive detector AMPTEK (USA). Crystallite size (D, Å) was evaluated using the Scherrer equation:

$$D = \frac{\lambda}{\beta \cos\theta}$$

Here λ is wavelength; β is angular broadening over 2θ; θ is Bragg angle. Broadening was determined by means of approximations using the Cauchy-Lorentz method according to equation $\beta = B - b$, where B is the integral width of the analytical line; b is the instrumental width, which was determined with respect to the lines related to quartz near the analytical lines. The reflections for the evaluation of broadening were chosen from the region of the least angles but with the highest intensity.

Electrochemical studies were carried out with the help of a Parstat 4000 potentiostat/galvanostat (Princeton Applied Research, USA) in a two-electrode cell with collector electrodes made of stainless steel and a Nafion separator. A 6 M KOH solution was used as the electrolyte.

Measurements were carried out using an asymmetric cell: the working electrode was a hybrid electrode material based on nanocomposites impregnated with potassium hydroxide, while counter-electrode was the initial MWCNT matrix. The capacitance of the electrode cell (C_{cell}, F/g) was determined from the area limited by the curves of cyclic voltammetry (CVA):

$$C_{cell} = \frac{\int I(U)\mathrm{d}U}{mv\Delta V} \quad (4)$$

Where the numerator is the area limited by the CVA curve in V–A coordinates; m is electrode mass, g; v is potential scanning rate, V/s; DV is the width of the potential window (the difference of potentials), V.

The capacities of working electrodes (C_{el}) were determined using equation

$$C_{el} = \frac{C_{cell} \cdot C_0}{C_0 - C_{cell}} \quad (5)$$

where C_0 is the capacitance of the counter-electrode.

RESUTLS AND DISCUSSION

Sample composition

Results of the analysis of MWCNTB/Co_3O_4 composite by means of OES are presented in Table 3. One can see that the experimentally determined cobalt content is close or practically equal to the calculated value (samples B13.1 and B14.1, respectively). For the B15.1 sample, a substantial excess of the experimentally determined Co content value over the calculated one may be due to more intense oxidation of MWCNT in the

TABLE 3

Results of optical emission analysis

Sample	Composition of the composite	Calculated Co concentration in NC, mass %	Experimentally determined Co concentration in NC, mass %
B13.1	MWCNT/Co_3O_4	5	3.31±0.02
B14.1	MWCNT/Co_3O_4	10	10.0±0.1
B15.1	MWCNT/Co_3O_4	15	48.0±0.4

air at increased temperature (4 h at 300 °C in the case under consideration) with relatively high (more than 10 mass %) cobalt content in the form of Co_3O_4, which is the catalyst of oxidation [17]. To reveal the reasons for non-proportional divergence between the values of cobalt concentration, additional experiments are necessary.

It should only be stressed that the mass of NC containing mixed cobalt-zinc oxide (total metal content 10 mass %) decreases after heating under similar conditions (see Table 2). The effect is non-monotonously dependent on the Co/Zn ratio but generally, it decreases noticeably with an increase in this ratio. It was confirmed by means of XFlA (see Table 2) that Co/Zn ratios in M1–M4 samples correspond to those prescribed during the synthesis of the composite and remain almost unchanged during TT. So, oxide fillers indeed act as the catalysts of the oxidation of carbon matrices.

Phase compositions of nanostructured composites

According to the data of X-ray spectra (Fig. 1), the major impurity elements in MWCNT are chlorine (2.62 keV), calcium (3.69 keV), titanium (4.51 keV) and chromium (5.41 keV), which are present in trace amounts and are detected also in the resulting NC. A strong alpha-beta pair of iron lines (6.40 and 7.06 keV) is the result of scattering by the samples of the radiation from the X-ray tube used in the apparatus, argon (2.96 keV) is a natural component of the air. The target elements – cobalt (6.93 and 7.65 keV) and zinc (8.64 and 9.57 keV) are represented in the spectra by alpha-beta pairs of lines. A decrease in the intensity of chlorine line in B13–B15 composites in comparison with the MWCNT sample and the absence of sulphur (2.31 keV) in M1–M4 composites provide evidence of the high-quality washing

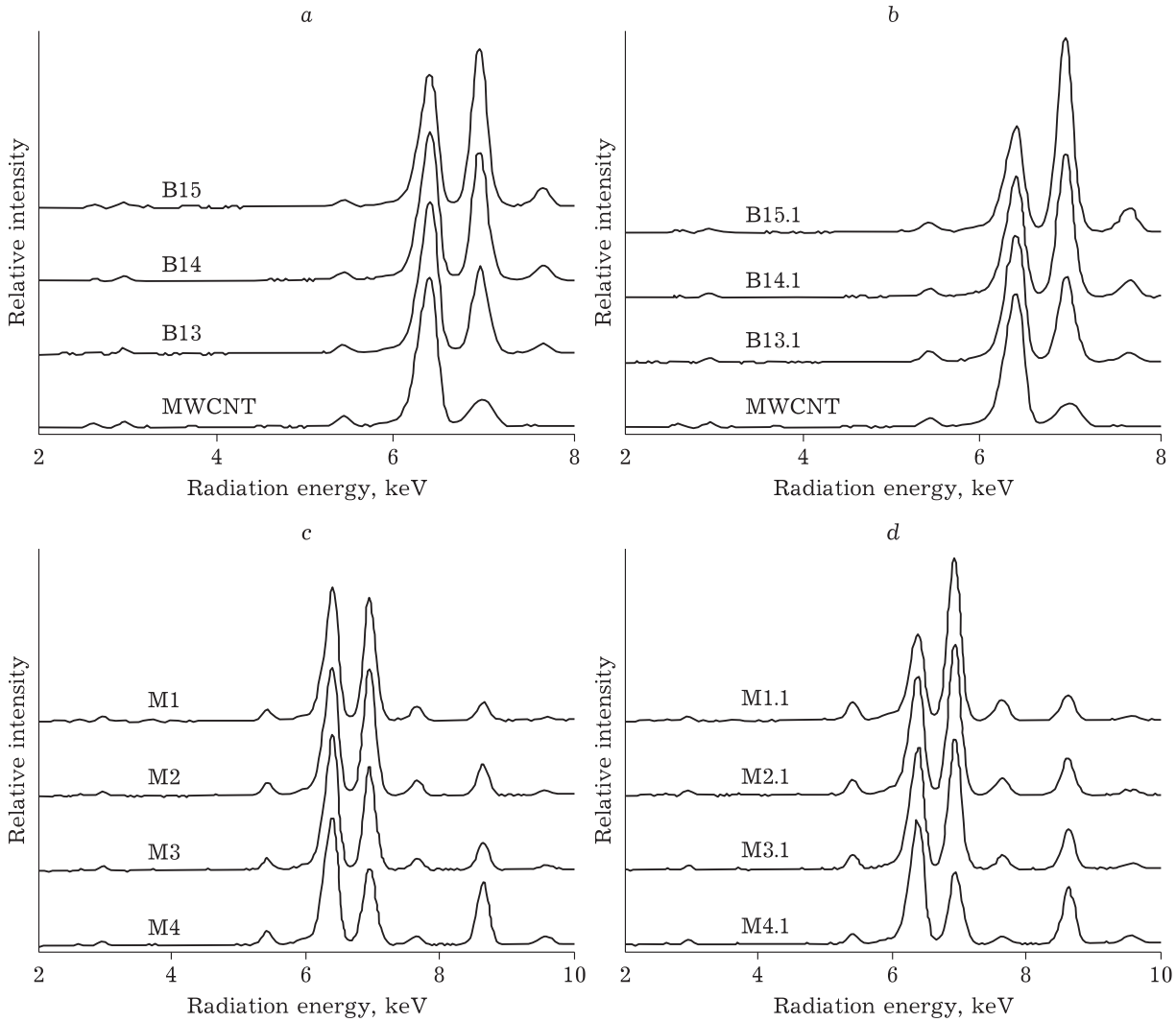

Fig. 1. X-ray spectra: *a* – MWCNT and B13–B15 composites before thermal treatment (TT); *b* – MWCNT and B13.1–B15.1 composites after TT; *c* –M1–M4 composites before TT; *d* –M1.1–M4.1 composites after TT.

of sodium chloride and sulphate formed during sample preparation.

It should be noted that after TT the intensity of lines in the X-ray spectra of both series of samples becomes somewhat higher. Some decrease in the intensity of iron lines is also noticeable. At the same time, for the samples of MWCNT/$Zn_xCo_{(1-x)}O_y$ series the ratio of cobalt to zinc line intensities in X-ray spectra does not change after TT (see Fig. 1, *c*, *d*).

According to the results of weighing (see Table 2), the loss of mass by samples M1–M4 during TT is 6.4 to 12.0 mass %. These differences are too large for simple dehydration of hydroxides. In addition to water removal, partial oxidation of cobalt (II) in the filler proceeds with the addition of oxygen, and this decreases possible mass losses even more. Actually, the fraction of dehydration in the total mass loss during TT is even smaller because a portion of the substance is present not in the form of hydroxide but in the form of mixed oxide $Co_xZn_{(1-x)}O_y$. So, the oxidation (burn-out) of the matrix should be considered as the major reason of a substantial increase in the fraction of metals in the composite after TT.

An increase in the intensity of metal lines in XRD spectra of the samples of both series (B and M) is due to an increase in metal concentration in the samples (see Fig. 1), which leads to the weakening of the scattering of iron tube radiation because of several reasons: first of all, due to an increase in the coefficient of radiation absorption by the sample; second, due to a decrease in the volume fraction of carbon matrix, since it is X-ray amorphous matrix that mainly scatters the radiation from the tube at the angle involved (120°), while metal-containing phases do not have diffraction reflections at this angle.

The diffraction patterns of the obtained NC of the B13–B15 series before and after TT are shown in Fig. 2. The ICDD bases available for authors do not contain any suitable versions for the identification of B15 sample (15 mass % Co) on the basis of diffraction patterns, so we may state that in this case some products poorly prone to identification are formed in the hydrolysis of cobalt salts in the presence of carbamide. The weakly pronounced peaks (~42.4, 46.0, 50.0, 54.8° over 2θ) most probably correspond to the complexes of cobalt and carbamide.

At the same time, thermal decomposition of the filler in these composites in the air leads to the formation of fine cobalt oxide Co_3O_4, which is indicated by the presence of broad peaks at 36.6, 46.8, 57.2, 77.0° over 2θ. With an increase in cobalt concentration in the composite material, the lines of cobalt oxides become more clearly pronounced.

Evaluation of crystallite size for B13–B15 samples gives 10–15 nm for the products of hydrolysis in the presence of carbamide, but after thermal decomposition, the crystallites become larger (15–20 nm) and exist in the form of spinel-type oxide (Co_3O_4).

Diffraction patterns of samples obtained as a result of the reaction between metal sulphates and sodium hydroxide in the aqueous medium (Fig. 3, *a*) are presented, in addition to the X-ray amorphous profile of scattering by the carbon matrix, by the reflections of $Co(OH)_2$ and ZnO; the intensities of the latter reflections changes regularly with changes in the composition of the samples.

The positions of the reflections of zinc oxide in the samples with different compositions (see Fig. 3, *b*) allow us to state definitely that it contains also a small amount of cobalt, so it is a mixed oxide. With an increase in cobalt content in the sample, the reflections of zinc oxide shift to larger angles because cobalt atoms have a smaller size than zinc atoms ($D(Co^{2+})$ = 0.72 E; $D(Zn^{2+})$ = 0.74 Å).

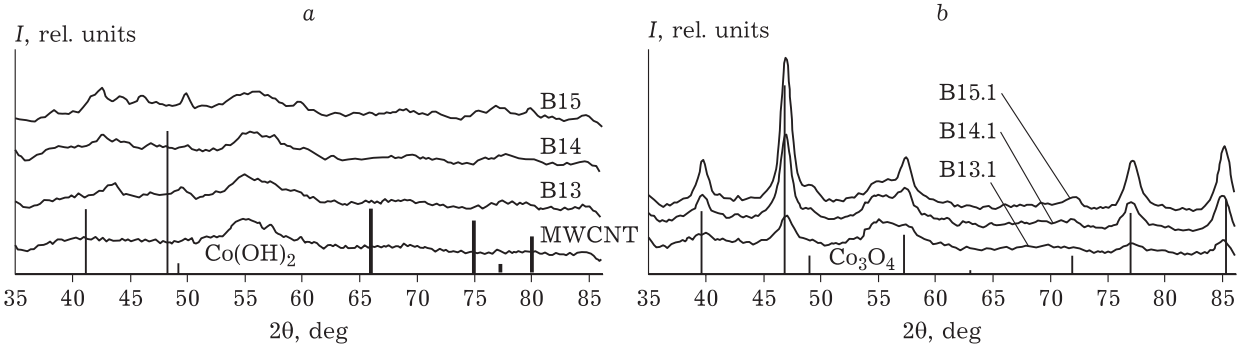

Fig. 2. Diffraction patterns: *a* – intermediate products (composite materials B13, B14, B15); *b* – final composites (B13.1, B14.1, B15.1). The line diagrams of $Co(OH)_2$ *(a)* and Co_3O_4 *(b)*.

The volume per one formula unit of ZnO (the structural type of wurtzite; a = 3.260 Å, c = 5.207 Å; PDF 46-1451) is 23.8 Å^3, while the volume per one formula unit of CoO (the structural type of NaCl; a = 4.260 E; PDF 43-1014) is 19.3 Å^3, which is smaller by 19 %. The observed maximal shift of

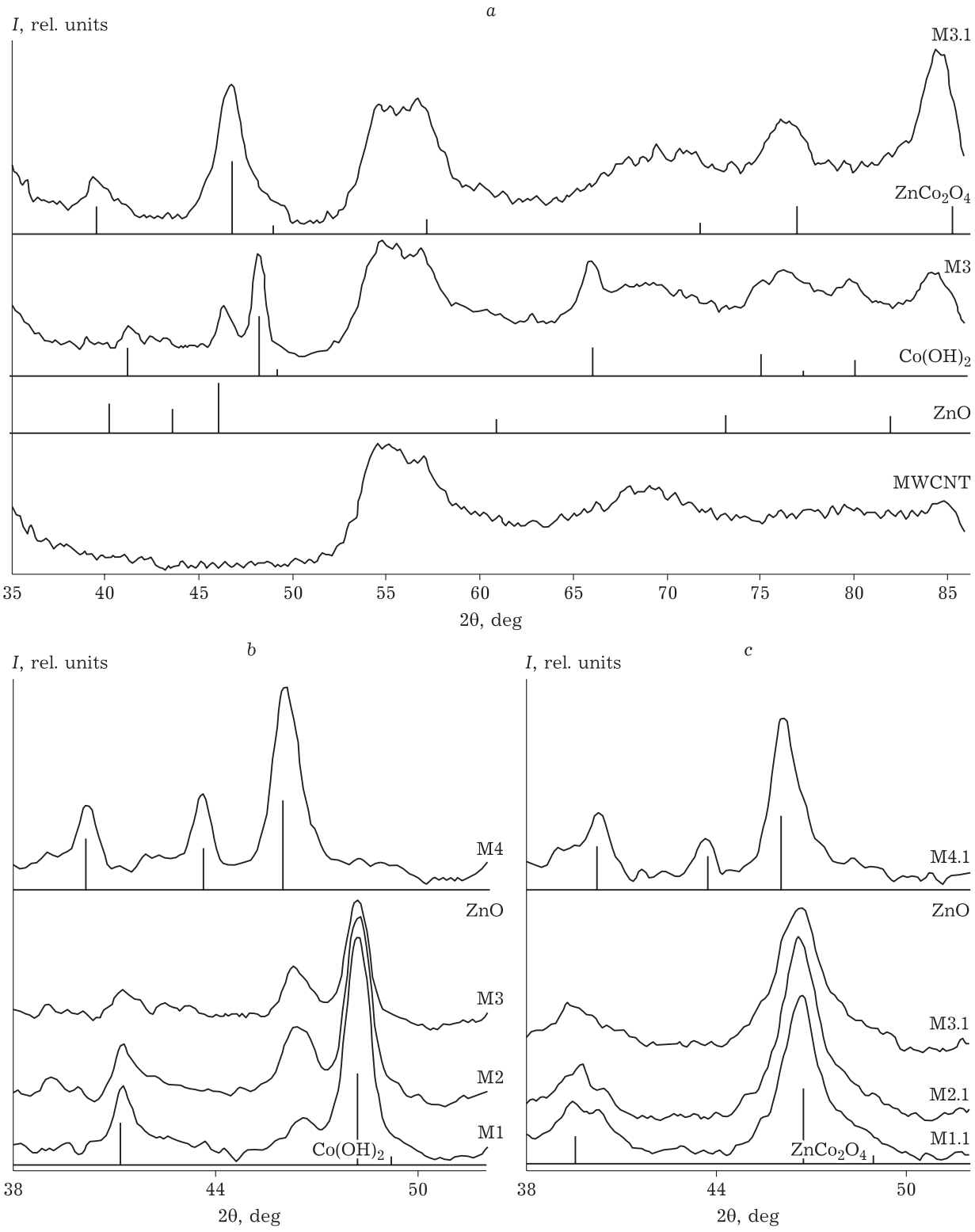

Fig. 3. Diffraction patterns of MWCNT and composites before TT (M3) and after TT (M3.1) (*a*); characteristic fragments of the diffraction patterns of nanocomposites before (*b*) and after TT (*c*) with different molar fractions of cobalt in the filler: 0.90 (M1 and M1.1); 0.75 (M2 and M2.1), 0.50 (M3 and M3.1); 0.25 (M4 and M4.1). Line diagrams of ZnO (*a*–*c*), $Co(OH)_2$ (*a*, *b*) и $ZnCo_2O_4$ (*a*, *c*).

the major reflection of the mixed oxide (101) is about 0.55° over 2θ, which corresponds to the change of interplanar distance by 1 %, while this value to the third power (as an averaged measure of volume) changes by 3 %. In the approximation of volume additivity during mixing (Vegard rule), the maximal content of cobalt in the mixed oxide may be estimated as 16 % – for M1 sample (the molar fraction of Co in the filler is 0.90). Незначительное Insignificant amount of Co may be also present in the mixed oxide of sample M4 with minimal cobalt content (molar fraction 0.25).

Cobalt (II) hydroxide in M1–M4 samples also may contain the second component, Zn, taking into account the isostructural nature of cobalt and zinc hydroxides (brucite type). However, its limiting possible content in $Co(OH)_2$ is small, so even in M1 sample (the molar fraction of Zn is 0.10) the amount of this metal is sufficient for the saturated solid solution of $Zn(OH)_2$ in $Co(OH)_2$ to be formed. The phase of mixed oxide is also formed, which is composed mainly of ZnO. So, the possible zinc content in the mixed hydroxide is substantially lower than 10 %. It is very difficult to detect the presence of zinc in the hydroxide and to determine its content because the parameters of $Co(OH)_2$ lattice may vary substantially according to the data presented in ICDD. One of the reasons is the possible partial oxidation of cobalt into the 3+ state. This phenomenon manifests itself very clearly for iron hydroxide, for which it is difficult to obtain the oxide corresponding to $Fe(OH)_2$.

One can see in the diffraction patterns (Fig. 3, *a*, *c*) that cobalt (II) hydroxide gets dehydrated as a result of TT and combines with zinc oxide forming zinc-cobalt spinel $ZnCo_2O_4$ ($ZnO \cdot Co_2O_3$) so that Co^{2+} ions are partially oxidized to Co^{3+}. Spinel content in M4 sample (the molar fraction of Co is 0.25) is not high, and its strongest reflection (311) is detected at the profile of the major reflection of the oxide (101) only as a shoulder from the side of larger angles; the (220) reflection is also observed at about 39.5° over 2θ. In other samples, the oxide is not visible. This means that the composition of the spinel phase is generally close to the composition of the samples, which is at first view in contradiction with the apparent constancy in the positions of spinel reflections in spite of substantial differences in composition.

This observed constancy is explained, first of all, by the close lattice parameters for Co_3O_4 and $ZnCo_2O_4$ (8.084 E, PDF 43-1004 and 8.094 E, PDF 23-1390, respectively). The difference in lattice parameters is only 0.1 %, and the maximal possible difference in diffraction angles is even smaller (several hundredths of a degree) because the compositions of the formed spinels occupy an intermediate position between pure Co_3O_4 and $ZnCo_2O_4$. For instance, the calculated excess of Co in $ZnCo_2O_4$ of M1.1 sample is 23 %, in M2.1 – 8 %, while in M3.1 – a small deficit of 17 %. The signs of the presence of zinc oxide are most noticeable in the latter sample.

The next essential moment is the incomplete formation of the regular crystal structure of spinels, which is seen in the complicated shape (a strong broadening in the lower part) of the diffraction profile. In this so-called proto-spinel phase, metal atoms have not yet occupied their positions in tetrahedral and octahedral cavities of the tightest three-layer packing composed of oxygen atoms. It should be noted that initial substances (zinc oxide and cobalt (II) hydroxide) are structurally akin to spinel. Metal atoms in them similarly occupy the cavities (only octahedral ones) in the oxygen packing (which is two-layer in this case).

So, the high degree of angular similarity of the profiles of diffraction scattering from spinels in M1–M3 samples with different compositions is not an obstacle to decide that they contain $Zn_xCo_{(1-x)}O_y$ spinel with x to y relations controlled by synthesis conditions. The major part of zinc may still be present in the zinc oxide phase, especially in M3 sample with the molar fraction of cobalt 0.50.

Investigation of composites by means of cyclic voltammetry

CVA curves from an asymmetric cell with the working electrode based on NC and counter-electrode based on the initial MWCNT matrix are presented in Fig. 4.

The appearance of voltage-current curves points to the absence of a clearly expressed contribution from pseudo-capacity due to slow oxidation-reduction reactions participated by Co_3O_4 into the total capacitance of the supercapacitor cell. The type of the dependence of specific capacitance on the rate of potential scanning (see Fig. 4) is practically identical for the electrodes based on MWCNT and on MWCNT/Co_3O_4 composite. The effect of an increase in the electric capacitance of the latter (about 1.25 times for the B14.1 sample, see Fig. 4, *b*) is only weakly dependent on the rate of potential scanning. This is evidence that the rate of oxidation-reduction

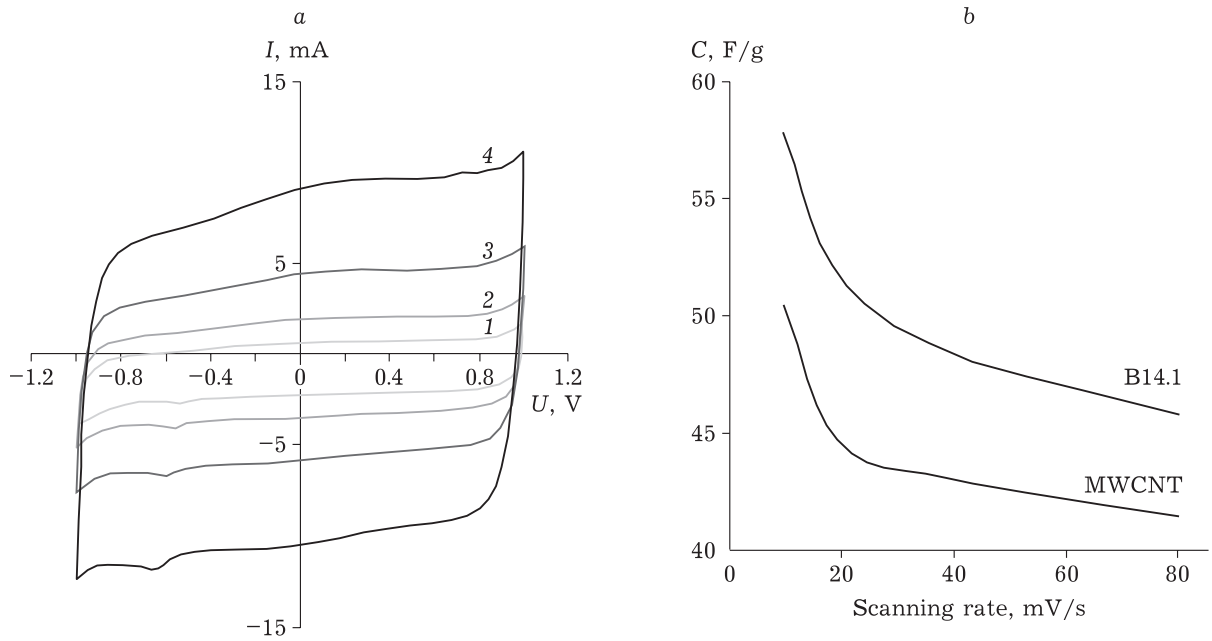

Fig. 4. *a* – CVA curves for the asymmetric cell with the MWCNT/Co_3O_4 working electrode (B14.1, the molar fraction of Co is 0.10). The rate of potential scanning, mV/s: 10 (*1*); 20 (*2*); 40 (*3*); 80 (*4*); *b* – dependences of the capacitance of electrode based on initial MWCNT matrix and composite MWCNT/Co_3O_4 (B14.1, the molar fraction of Co is 0.10) on the rate of potential scanning.

electrode reactions providing an increase in the capacitance of the electrodes based on NC is comparable with the rate of formation of the double electric layer on MWCNT electrodes.

The picture is somewhat different for electrode materials obtained according to the traditional scheme of the deposition of cobalt and zinc hydroxides, followed by thermal treatment (M1–M4 samples, Fig. 5). For the low zinc content in the composite (M1 sample, the molar fraction of Zn is 0.10), we obtained smooth voltage-current curves for M1 sample (see Fig. 5, *a*) and the curves with clearly pronounced pseudo-capacity effect for M1.1 sample (see Fig. 5, *b*). However, the type of dependences changes with an increase in zinc content in the filler. For instance, in NC samples with the molar fraction of Zn equal to 0.75, the voltage-current curves for M4 sample point to a substantial contribution from pseudo-capacity processes into the total capacitance of the electrode (see Fig. 5, *g*), while the curves for M4.1 sample turn out to be smooth (see Fig. 5, *h*), though the extreme points may be masked in the latter case due to several pseudo-capacity processes following one another.

It follows from the dependences of specific capacitance on the rate of potential scanning (Fig. 6) that an increase in capacitance for intermediate composites in comparison with the carbon matrix is achieved only at low scanning rates (10–20 mV/s), which may be due to the blockage of some pores on carbon surface and limitation of charging-discharging processes by relatively slow oxidation-reduction reactions in the filler. At the same time, an increase in specific capacitance for the composites after TT (see Fig. 6, *b*) is achieved within the whole range of the used rates of potential scanning, so that the highest effect (up to 1.5 times) is observed in the samples with the molar fraction ratio Co/Zn = 0.50 : 0.50 (M3.1 sample) in the filler. It may be assumed that thermal treatment involves compaction of the nanoparticles of mixed oxide in zinc cobaltate ($ZnCo_2O_4$), with partial elimination of the blockage of carbon matrix surface. The formation of the ordered $ZnCo_2O_4$ phase promotes more rapid progress of oxidation-reduction reactions in the filler because specific capacitance starts to decrease with further increase in zinc content.

CONCLUSION

Investigation results showed that the hydrolysis of cobalt (II) salts in the presence of carbon matrix and carbamide leads to the formation of nanocomposite in which the filler is a complicated mixture of hydroxides, carbonates, and carbamide complexes of cobalt. After thermal treatment at 300 °C in air, these compounds are transformed into nano-

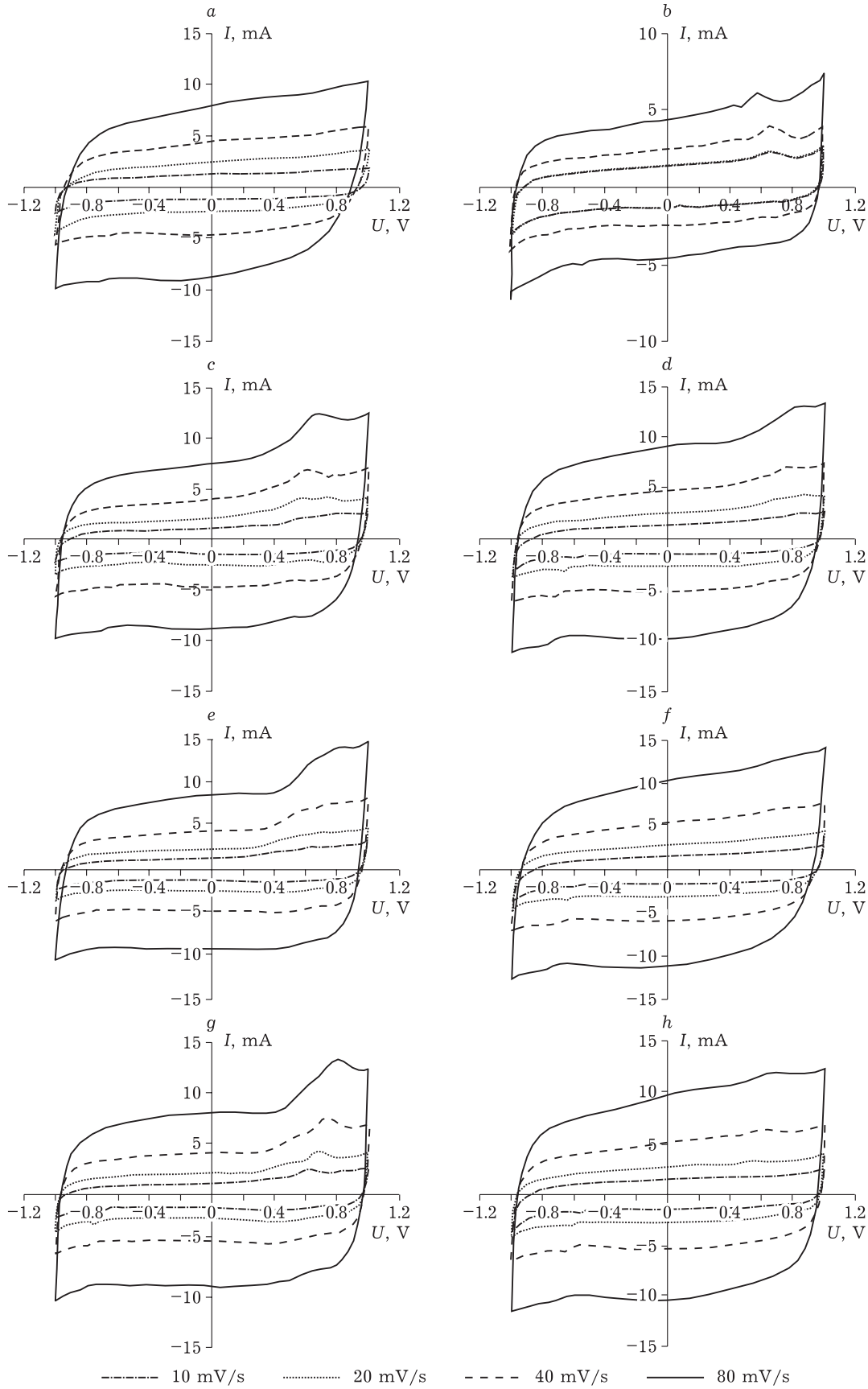

Fig. 5. CVA curves for the asymmetric cell with the working electrode based on M1–M4 composites *(a, c, e, g)* and M1.1–M4.1 *(b, d, f, h)* for different rates of potential scanning, mV/s: 10 (*1*); 20 (*2*); 40 (*3*); 80 (*4*).

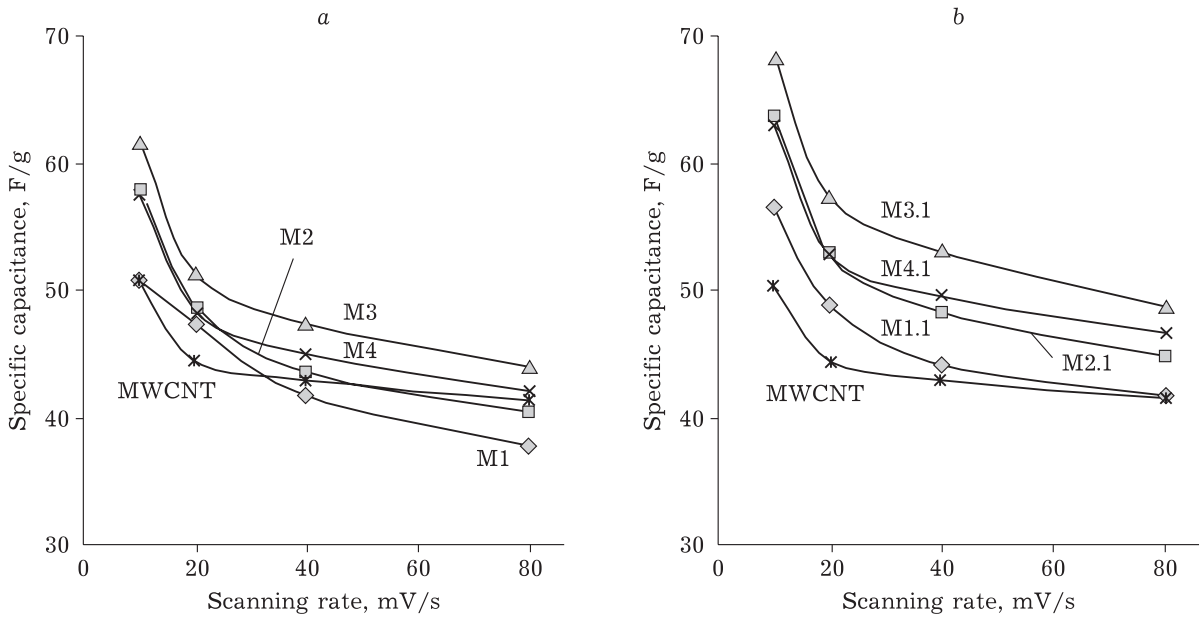

Fig. 6. Dependence of the specific capacitance of the electrode based on initial MWCNT matrix and electrodes based on composites M1–M4 *(a)* and M1.1–M4.1 *(b)* on potential scanning rate.

sized cobalt (II, III) oxide. In the case of sufficiently high Co_3O_4 content in the composite, thermal treatment at 300 °C is accompanied by enhancement of the partial oxidation of carbon matrix.

The specific electric capacitance of nanostructured composite based on MWCNT filled with nano-sized cobalt oxide is 1.1–1.25 times higher than the specific capacitance of initial MWCNT.

The treatment of cobalt and zinc salts with the solution of sodium hydroxide in the presence of the carbon matrix leads to the formation of a mixture of zinc oxide and cobalt hydroxide. Thermal treatment of the resulting mixtures with the molar fraction of cobalt not less than 0.50 leads to the formation of spinel-type nano-sized zinc cobaltate $Zn_xCo_{(1-x)}O_y$. The use of electrode materials based on zinc cobaltate allows an increase in the specific capacitance of supercapacitors by a factor of 1.5 with respect to the materials based on carbon matrix, which saves cobalt as a tight resource for the manufacture of the supercapacitor.

Acknowledgements

The work was carried out with financial support within the projects of the Ministry of Education and Science (V.46.3.1) and RFBR (20-43-420017/20), using the equipment of the Shared Equipment Centre at the FRC CCC SB RAS (Kemerovo).

The authors thank A. S. Chichkan (BIC SB RAS, Novosibirsk), E. S. Mikhailova for MWCNT samples, and R. P. Kolmykov for carrying out the elemental analysis.

REFERENCES

1 Gonzalez A., Goilolea E., Barrena A., Mysyk R., Review of supercapacitors: Technologies and materials, *Renewable and Sustainable Energy Rev.*, 2016, Vol. 58, P. 1189–1206.

2 Yu A., Chabot V., Zhang J., Electrochemical Supercapacitors for Energy Storage and Delivery: Fundamentals and Applications, Boca Raton: CRC Press, 2013. 348 p.

3 Sk M. M., Yue C. Y., Ghosh K., Jena R. K., Review of advances in porous nanostructured nickel oxide and their composite electrodes for high-performance supercapacitors, *J. Power Sources*, 2016, Vol. 308, P. 121–140.

4 Lee K. K., Chin W. S., Sow C. H., Cobalt-based compounds and composites as electrode materials for high-performance electrochemical capacitors, *J. Mater. Chem. A*, 2014, Vol. 2, P. 17212–17248.

5 Larichev T. A., Fedorova N. M., Zakharov Yu. A., Simenyuk G. Yu., Pugachev V. M., Dodonov V. G., Kachina E. V., Mikhailova E. S., Synthesis of a carbon/$NiCo_2O_4$ material for a supercapacitor by thermal decomposition of mixed cobalt-nickel hydroxides, *Chemistry for Sustainable Development*, 2018, Vol. 26, No. 6, P. 619–624.

6 Zakharov Yu. A., Kachina E. V., Fedorova N. M., Larichev T. A., Simenyuk G. Yu., Pugachev V. M., Dodonov V. G., Zaytseva E. Yu., Yakubik D. G., Mikhailova E. S., Morphology and electrochemical properties of nanostructured composite $Co_xNi_{(1-x)}(OH)_2$/MWCNT based on carbon nanotubes, *Chemistry for Sustainable Development*, 2019, Vol. 27, No. 6, P. 590–597.

7 Lei H., Shi Z., Wang X., Wang T., Ai J., Shi P., Xue R., Guo H., Yang W., Solvothermal synthesis of pompon-like nickel-cobalt hydroxide/graphene oxide composite for high-performance supercapacitor application, *Colloid and Surface A*, 2018, Vol. 548, P. 76–85.

8 Wang G., Shen X., Horvat J., Wang B., Liu H., Wexier D., Yao J., Hydrothermal synthesis and optical, magnetic and supercapacitance properties of nanoporous cobalt oxide nanorods, *J. Phys. Chem. C*, 2009, Vol. 113, P. 4357–4361.

9 Yan J., Wei T., Qiao W., Shao B., Zhao Q., Zhang L., Fan Z., Rapid microwave-assisted synthesis of graphene nanosheet/

Co_3O_4 composite for supercapacitor, *Electrochem. Acta*, 2010, Vol. 55, P. 6973–6978.
10 Bai Y., Liu M., Sun J., Gao L., Fabrication of Ni-Co binary oxide/reduced graphene oxide composite for high capacitance and cyclicity as efficient electrode for supercapacitors, *Ionics*., 2016, Vol. 22, P. 535–544.
11 Shaw W. H. R., Bordeaux J. J., The decomposition of urea in aqueous media, *J. Amer. Chem. Soc.*, 1955, Vol. 77, No. 18, P. 4729–4733.
12 Sugimoto T., Monodispersed Particles, Elsevier Science, 2001. P. 235–238.
13 Qiu Y., Metal-urea complex – A precursor to metal nitrides, *J. Am. Ceram. Soc*., 2004, Vol. 87, No. 3, P. 352–357.
14 Lee K. K., Chin W. S., Sow C. H., Cobalt-based compounds and composites as electrode materials for high-performance electrochemical capacitors, *J. Mater. Chem. A*, 2014, Vol. 2, P. 17212–17248.
15 Bao F. X., Wang X. F., Zhao X. D., Wang Y., Ji Y., Zhang H. D., Liu X. Y., Controlled growth of mesoporous $ZnCo_2O_4$ nanosheet arrays on Ni foam as high-rate electrodes for supercapacitors, *RSC Advances*, 2014, Vol. 4, P. 2393–2397.
16 Wang Q. H., Du J. L., Zhu Y. X., Yang J. Q., Chen J., Wang C., Li L., Jiao L. F., Surface fabrication and super capacitive properties of mesoporous zinc cobaltite microspheres, *J. Power Sources*, 2015, Vol. 284, P. 138–145.
17 Chigrin P. G., Lebukhova N. V., Ustinov A. Yu., Structural transformations of $CuMoO_4$ during the catalytic oxidation of carbon [in Russian], *Kinetika i Kataliz*, 2013, Vol. 54, No. 1, P. 1–6.